IOP Publishing Nanotechnology
Nanotechnology **25** (2014) 165201 (7pp) doi:10.1088/0957-4484/25/16/165201

# Improved performance of graphene transistors by strain engineering

**V Hung Nguyen[1,2], Huy-Viet Nguyen[2] and P Dollfus[3]**

[1] L_Sim, SP2M, UMR-E CEA/UJF-Grenoble 1, INAC, F-38054 Grenoble, France
[2] Center for Computational Physics, Institute of Physics, Vietnam Academy of Science and Technology, PO Box 429 Bo Ho, 10000 Hanoi, Vietnam
[3] Institut d'Electronique Fondamentale, UMR8622, CNRS, Université Paris Sud, F-91405 Orsay, France

E-mail: hung@iop.vast.ac.vn

Received 20 December 2013, revised 12 February 2014
Accepted for publication 3 March 2014
Published 26 March 2014

## Abstract

By means of numerical simulation, in this work we study the effects of uniaxial strain on the transport properties of strained graphene heterojunctions and explore the possibility of achieving good performance of graphene transistors using these hetero-channels. It is shown that a finite conduction gap can open in the strain junctions due to strain-induced deformation of the graphene bandstructure. These hetero-channels are then demonstrated to significantly improve the operation of graphene field-effect transistors (FETs). In particular, the ON/OFF current ratio can reach a value of over $10^5$. In graphene normal FETs, the transconductance, although reduced compared to the case of unstrained devices, is still high, while good saturation of current can be obtained. This results in a high voltage gain and a high transition frequency of a few hundreds of GHz for a gate length of 80 nm. In graphene tunneling FETs, subthreshold swings lower than 30 mV/dec, strong nonlinear effects such as gate-controllable negative differential conductance, and current rectification are observed.

Keywords: graphene, strain, field-effect-transistor, simulation

(Some figures may appear in colour only in the online journal)

## 1. Introduction

Graphene, due to its outstanding electronic properties [1], is expected to be an excellent candidate for advanced applications in future electronics [2, 3]. In particular, graphene field-effect transistors (FETs) take advantage of the high carrier mobility [4, 5] and high critical current density [6], which makes them suitable for operating in high-frequency ranges [2]. Intrinsic cut-off frequencies of a few hundreds of GHz [7, 8] and a record maximum oscillation frequency of 70 GHz [9] in graphene devices have been reported recently. However, for practical applications, graphene transistors still have serious drawbacks associated with the lack of an energy bandgap and a poor saturation of the current [2]. The former makes it difficult to turn off the current, leading to a small ON/OFF current ratio, typically lower than ten [10]. The latter results in a small voltage gain and a consequent power loss when the devices are integrated in a circuit. So far, many attempts at bandgap engineering in graphene [11–15] have been made to overcome these limitations. A common technique consists in cutting the 2D graphene sheets into 1D narrow nanoribbons [11]. To open a bandgap in 2D graphene sheets, some prominent options are Bernal-stacking of graphene on hexagonal boron nitride substrates [12], nitrogen-doped graphene [13], graphene nanomesh lattices [14] and Bernal-stacking bilayer graphene [15]. However, each technique has its own issues. For instance, graphene nanoribbon (GNR) devices require a narrow width with a good control of edge disorder [16]. Graphene nanomesh lattices have the same requirement concerning good control of the lattice of nanoholes and the disorder [17], while the bandgap opening in bilayer graphene may not be large enough to achieve a sufficiently high ON/OFF ratio in transistors for digital applications [18]. Other proposed methods still need experimental verification and realization.

In addition to being attractive for electronics, graphene also shows remarkable mechanical properties [19]. It was

 

experimentally demonstrated that graphene's mechanical endurance far exceeds that of any other available material at the moment, making it a promising candidate for flexible electronics (for further information see the recent review [20]). For instance, a graphene sheet on an unstretched polydimethylsiloxane substrate can endure and show good recovery of sheet resistance after 6% stretching [21]. On a pre-stretched polydimethylsiloxane substrate, graphene even showed stable sheet resistance up to ∼11%, and there was only a one order change in this resistance up to ∼25% stretching. In fact, strain engineering offers a wide range of opportunities for modulating the electronic properties of graphene nanostructures. In particular, the bandgap in armchair GNRs has a linear strain-dependence under weak strain, whereas it presents periodic oscillations at large strain [22]. For a zigzag GNR, strain can change the spin polarization at the ribbon edges, and therefore modulate its bandgap. In a 2D monolayer graphene, a finite gap can open under very large shear strain [23]. Otherwise, the bandgap may remain close to zero but the Dirac points are displaced [24, 25]. Many interesting electrical, optical and magnetic properties induced by strain have been also reported, e.g., in [24, 26–32].

In the present work, we focus on the effects of uniaxial strain applied in a 2D monolayer graphene sheet and explore the possibility of using a strained/unstrained hetero-channel (see figure 1) to achieve good operation of graphene FETs. Actually, local strain has been realized in experiments [26, 33–38] and theoretically demonstrated to improve the electrical performance of various graphene devices [24, 39–42]. For instance, the local strain has been shown to enhance the ON current in a GNR tunneling FET by a factor of ten [39] and to increase the transport gap in strained GNR junctions [42]. We will demonstrate here that the use of a strained heterostructure with a moderately small strain of 5% can greatly improve the performance of graphene FETs with respect to a high ON/OFF ratio and good saturation of the current in normal transistors; and low subthreshold swing and strong nonlinear effects in tunneling devices.

It should be noted that in this work, as commonly used for ambipolar devices, our definition of the ON/OFF current ratio is not the standard definition for CMOS operation. It is arbitrarily defined here for a specific value of drain voltage $V_{ds}$ (typically $V_{ds} = 0.1, 0.2, 0.3$ or $0.4$ V) as the ratio of the current for $V_{gs} = 0.35$ V to the minimum current at the so-called Dirac point, the position of which is usually dependent on $V_{ds}$.

## 2. Approach

Our model is based on a nearest-neighbor tight-binding Hamiltonian as in [43]. The application of a uniaxial strain along the $Ox$ (transport) direction causes the following changes in the C–C bond vectors:

$$\begin{aligned} r_x &\to (1+\sigma)\, r_x \\ r_y &\to (1-\nu\sigma)\, r_y \end{aligned} \qquad (1)$$

where $\sigma$ represents the strain and $\nu \simeq 0.165$ is the Poisson ratio [44]. The hopping parameter between atoms $i$ and $j$ is defined in [43] as $t_{ij} = t_0 \exp\left[-3.37\left(r_{ij}/r_0 - 1\right)\right]$, where $r_{ij}$

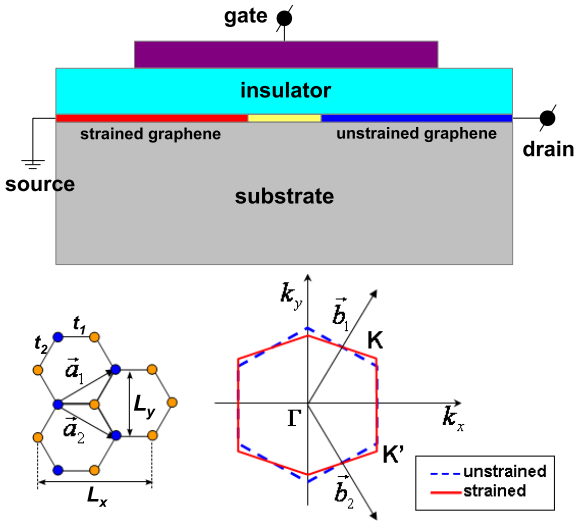


**Figure 1.** Schematic of the graphene FETs simulated in this work (top) and a graphene lattice together with its first Brillouin zone (bottom). The channel of the simulated device is based on strained graphene heterostructures. The yellow zone in the top figure indicates the transition region between strained and unstrained sections. At the bottom, the left panel shows the honeycomb structure with the lattice vectors $\mathbf{a}_1$ and $\mathbf{a}_2$. $L_{x,y}$ are the lengths of the unit cell (four atoms per cell) along the $Ox$ and $Oy$ directions, respectively. The right panel shows the Brillouin zones, showing the change in Dirac points ($\mathbf{K}$ and $\mathbf{K}'$) with uniaxial strains applied along the $Ox$-axis (transport direction).

is their bond length, while the hopping energy $t_0 = -2.7$ eV and the bond length $r_0 = 0.142$ nm in the unstrained case. Therefore, there are two different hopping parameters $t_{1,2}$ along the armchair and zigzag directions, respectively, in the strained graphene (see in figure 1). This tight-binding Hamiltonian is solved in the ballistic limit using the Green's function technique, self-consistently with Poisson's equation (for more details, see [45]). After the self-consistency is reached, the current is computed from the Landauer equation as

$$J = \frac{e}{\pi h}\int_{\mathrm{BZ}} \mathrm{d}k_y \int_{-\infty}^{\infty} \mathrm{d}\epsilon \mathcal{T}\left(\epsilon, k_y\right)\left[f_{\mathrm{S}}\left(\epsilon\right) - f_{\mathrm{D}}\left(\epsilon\right)\right] \qquad (2)$$

where $f_{\mathrm{S(D)}}(\epsilon)$ is the source (drain) Fermi distribution function, $\mathcal{T}(\epsilon, k_y)$ is the transmission coefficient and the integral over the wavevector $k_y$ is performed in the first Brillouin zone.

In our simulated devices schematized in figure 1, the gate of length 80 nm covers symmetrically both sides of the hetero-channel with a transition zone of ∼9 nm between unstrained and strained sections. The tensor strain in this transition zone is simply modeled as a linear function of position along the transport direction. Actually, we find, similar to what was reported in [42], that the transition region has important effects on the transport only if the length is short, i.e., smaller than about 5–6 nm. Hence, the choice of this simple model is reasonable due to the fact that this region has no significant effect on the transport with lengths of 9 nm or larger and there is no significant difference between our results and those obtained using other more sophisticated models, such as in [42]. We assume the doping concentration

$N_D = 10^{13}$ cm$^{-2}$ in the source and drain access regions and the gate stack is made of high-$\kappa$ insulator [10]. We consider in this work two typical devices: normal FET (nFET), where the source and drain access regions are both n-doped, and tunneling FET (TFET), where the drain is p-doped.

## 3. Results and discussion

First, let us analyze the basic transport properties of strained/unstrained graphene heterostructures. Solving the tight-binding Hamiltonian for strained graphene, we obtain the energy bands:

$$E^2(\mathbf{k}) = t_1^2 + 4t_2^2 \cos^2\left(\theta_y\right) \pm 4t_1 t_2 \cos\left(\theta_x\right) \cos\left(\theta_y\right) \quad (3)$$

where $\theta_{x(y)} = k_{x(y)} L_{x(y)}/2$, with the length $L_{x(y)}$ of unit cell as indicated in figure 1. Hence, the bandgap of uniformly strained graphene remains zero at $k_x = 2n\pi/L_x$ and $\cos\left(\theta_y\right) = \pm t_1/2t_2$ but the Dirac points are displaced under the effect of strain, as illustrated schematically in figure 1. This does not change the zero-conduction-gap characteristic of the graphene channel (see figure 2(a)) when we consider the conductance as a function of energy. However, in strained/unstrained heterostructures, we notice a very interesting phenomenon: the appearance of a finite conduction gap, which increases monotonically when increasing the strain (see figure 2(b)). This phenomenon is explained as follows. For a given $k_y$-mode, graphene has an energy gap defined as $E_{\text{gap}}(k_y) = 2|2t_2|\cos(\frac{k_y L_y}{2})| - t_1|$. Because of the shift of Dirac points induced by strain, as further illustrated by the plot of the conduction-band edge versus $k_y$ in the inset of figure 2(b), there is always a finite energy gap $E_{\text{gap}}^{\text{het}}(k_y)$ of transmission in the strained heterostructure. The value of this gap is the maximum of $E_{\text{gap}}(k_y)$ in the strained and unstrained graphene sections. Therefore, a finite gap of conductance occurs (see figure 2(a)) and is determined by the minimum value of $E_{\text{gap}}^{\text{het}}(k_y)$ when varying $k_y$ in the whole Brillouin zone: $E_{\text{cond.gap}} = 2|\frac{t_1 - t_2}{t_0 + t_2} t_0|$. This conduction gap is of course dependent on strain. For instance, it reaches about 360 meV for $\sigma = 5\%$ and can have a higher value for larger strains (see figure 2(b)). Similar properties of strained GNR junctions have also been discussed in [42]. It is important to keep in mind that, in conventional semiconductor devices, the finite bandgap of the channel is the key property responsible for the transport gaps (conduction gaps), and hence offers the possibility of switching off the current (to achieve high ON/OFF current ratio). Although there is no bandgap in either strained or unstrained graphene sections, here, the conduction-gap opening due to the shift of the Dirac point has the same effect and is suggested to be able to improve the performance of graphene FETs.

It has been shown [46, 47] that there are three components that contribute to the current in graphene nFETs: thermionic transmission in the energy regime higher than the gate-induced potential barrier, chiral tunneling through the barrier, and band-to-band tunneling taking place between the valence band in the source and the conduction band in the drain. While the band-to-band tunneling has an important contribution at high $V_{ds}$, which leads to a poor current saturation, the contribution

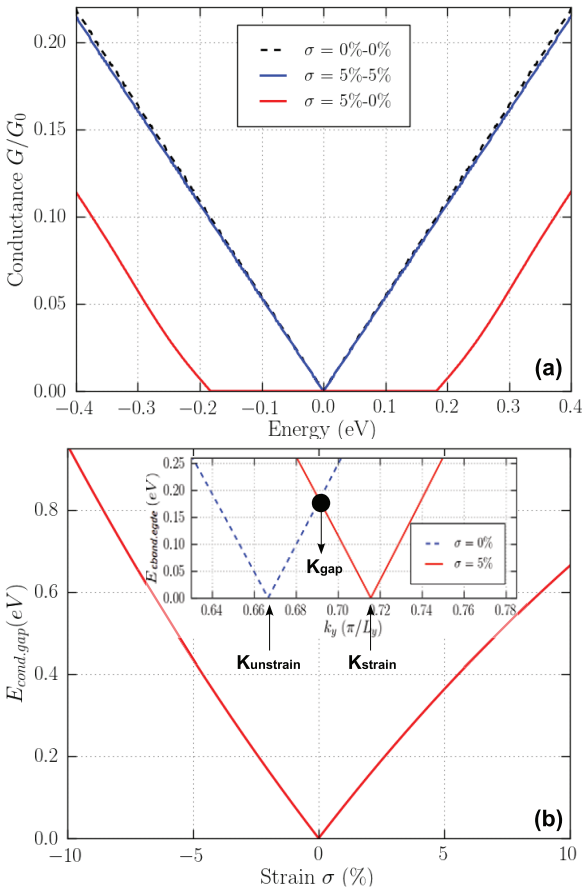


**Figure 2.** Conductance ($G_0 \equiv e^2 W/hL_y$) as a function of energy and evolution of the conduction gap in strained graphene heterostructures. The comparison of the conductance in unstrained, uniformly strained and strained heterostructures is shown in (a). The conduction gap as a function of strain in the heterostructures is displayed in (b), while the inset shows the edge of the conduction bands versus wavevector $k_y$.

of the other two components results in a high OFF current (low ON/OFF current ratio) in gapless graphene devices. Hence, the use of a gapped graphene channel is necessary to solve these issues. We first focus on the possibility of using a strained/unstrained graphene channel to improve the performance of graphene nFETs. We find, as displayed in figure 3(a), that when increasing the strain (or conduction gap), the OFF current is strongly reduced and, by defining arbitrarily the ON current as the current obtained at $V_{gs} = 0.35$ V, the ON/OFF current ratio increases significantly to over $10^5$ for $\sigma = 5\%$. Such a high ratio seems to be at variance with what was shown for bilayer graphene [18] and graphene nanomesh FETs [47], where an energy gap of ~300 meV is not enough to switch off the current efficiently, i.e., to obtain a large ON/OFF ratio. This may be because, in these devices, the energy gap occurs locally in the gated region and is, therefore, not sufficient to suppress the thermionic and/or band-to-band tunneling components. The situation here is different and can be explained as follows. In fact, the transport modes $k_y$ that contribute significantly to the current are the values $k_y$ in/around the range from $K_{\text{unstrain}}$ to $K_{\text{strain}}$ (see the inset of figure 2(b)). Far from this range to the left and to the right,

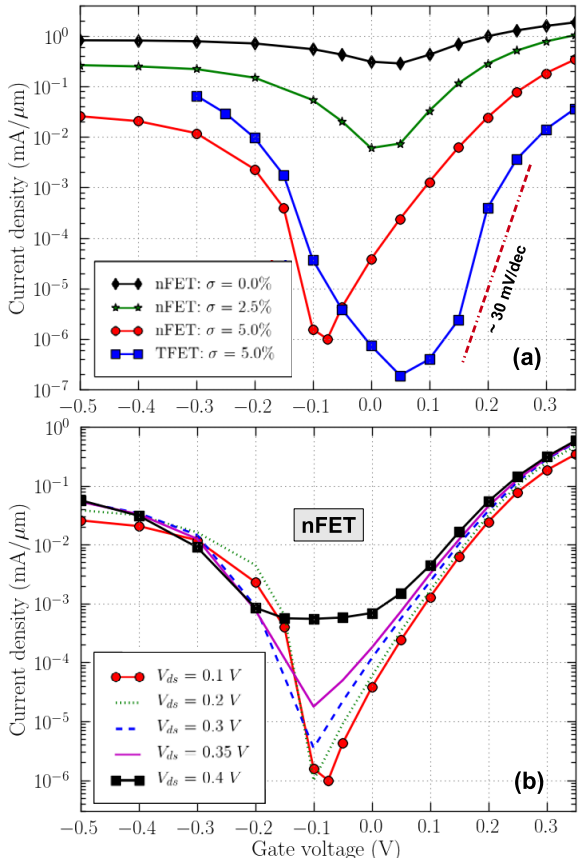


**Figure 3.** $I$–$V_{gs}$ characteristics of simulated graphene FETs at $V_{ds} = 0.1$ V with different strains (a) and for $\sigma = 5\%$ with different $V_{ds}$ (b).

the energy gap $E_{gap}(k_y)$ in the strained (source and half of the gated zone) and unstrained (drain and half of the gated zone) graphene sections, respectively, is too large, which very strongly suppresses the corresponding current component even in the ON state. Close to $k_y = K_{unstrain}$ or $K_{strain}$, the energy gap mentioned is still large, but the corresponding current component starts to have a significant contribution to the ON current, while it remains almost negligible in the OFF state. For other modes $k_y$, e.g., around $K_{gap}$, the energy gap of $\sim E_{cond.gap}$, though smaller than the gap of modes discussed above, occurs along the whole channel and is thus enough to switch off the corresponding component of current in the OFF state, as illustrated by the pictures of local density of states and transmission coefficient in figure 4 for $V_{ds} = 0.2$ V. The combined effect of these $k_y$-dependent energy gaps (discussed further below) makes the ON/OFF current ratio very large. We notice that this large ON/OFF ratio is obtained at the price of a reduced ON current. In particular, the current at $V_{gs} = 0.35$ V for $\sigma = 5\%$ decreases by a factor of about five, compared to the unstrained case. This reduction is however not much and is similar to that in other gapped graphene devices, e.g., see in [47].

Next, we investigate the operation of graphene TFETs using the same strained hetero-channel. The conventional TFETs, besides being able to offer a high ON/OFF current ratio, have an additional advantage of having steep subthreshold swings lower than the thermally limited value of 60 mV/dec [48]. This good performance, in principle, cannot be achieved with a gapless channel as in unstrained graphene devices. Using the strained hetero-channel, as shown in figure 3(a), an ON/OFF current ratio higher than $10^5$ is also achieved, while the subthreshold swing can reach a value smaller than 30 mV/dec. All the results obtained demonstrate that strained hetero-channels are excellent candidates for graphene devices in electronic applications.

We now move on to explore the influence of $V_{ds}$. In figure 3(b), we show $I$–$V_{gs}$ curves obtained in graphene nFETs for different $V_{ds}$. Interestingly, it is shown that a very high ON/OFF current ratio can still be achieved for high $V_{ds}$ up to about 0.3 V. Beyond this value of $V_{ds}$, the OFF current increases more rapidly and the ON/OFF ratio is hence reduced, but it still reaches a value of $\sim 10^3$ at $V_{ds} = 0.4$ V. This can be understood by looking at the pictures of local density of states and the transmission coefficient in figure 4. Note that the conduction/valence band edges with respect to the neutrality point are defined from equation (3) as $E_{edge}(k_y) = \pm \left| 2t_2 \cos\left(\frac{k_y L_y}{2}\right) - t_1 \right|$, respectively, whose $k_y$-dependences are different in the unstrained and strained graphene sections, as illustrated in the inset of figure 2(b) for the conduction-band edges. The energy window between the edges of valence bands and those of conduction bands defines the energy gaps of the LDOS and hence the gaps of the transmission coefficient shown in figure 4. Again, for $k_y$ around $K_{gap}$, the energy gaps in the source, gated and drain regions are merged together at $V_{ds}$ lower than 0.3 V, which forms a large enough conduction gap to strongly suppress the corresponding current component. For $k_y$ around $K_{strain}$ (similarly, for $k_y$ around $K_{unstrain}$), the energy gaps in the gated and drain regions are also merged together, and thus efficiently suppress the current. This explains the small OFF current obtained for $V_{ds}$ lower than 0.3 V. The situation changes suddenly at high $V_{ds}$ when the band-to-band tunneling comes into play. Indeed, as seen in figure 4 for $V_{ds} = 0.4$ V, the energy gap in the drain is separated from the others and the band-to-band tunneling has an important contribution to the current. This results in the rapid increase of the OFF current with $V_{ds}$ shown in figure 3(b).

In the negative range of $V_{gs}$, when the channel is p-doped, it has been shown in [46] that a pseudo-saturation of current or even a negative differential conductance (NDC) can be observed, which was explained by the reduction of chiral tunneling when increasing $V_{ds}$, together with the limited contribution of thermionic/band-to-band currents. Similar effects are also observed in our simulated devices in the range of $V_{gs}$ from $-0.4$ to $-0.05$ V. Because of the strong effect of the energy gaps mentioned, a strong NDC behavior with a peak-to-valley ratio of approximately six is even observed, as shown in the $I$–$V_{ds}$ curve presented in figure 5 for $V_{gs} = -0.2$ V. The saturation behavior is also achieved in the n-branch (very positive $V_{gs}$), where the thermionic current is dominant (see the further discussions below). Additionally, it is remarkable to notice that in this regime, although reduced compared to the unstrained graphene FETs, the transconductance $g_m$ of the strained hetero-channel devices is still high. In particular, the transconductance has a value of $\sim 4.3$ mS $\mu m^{-1}$ for

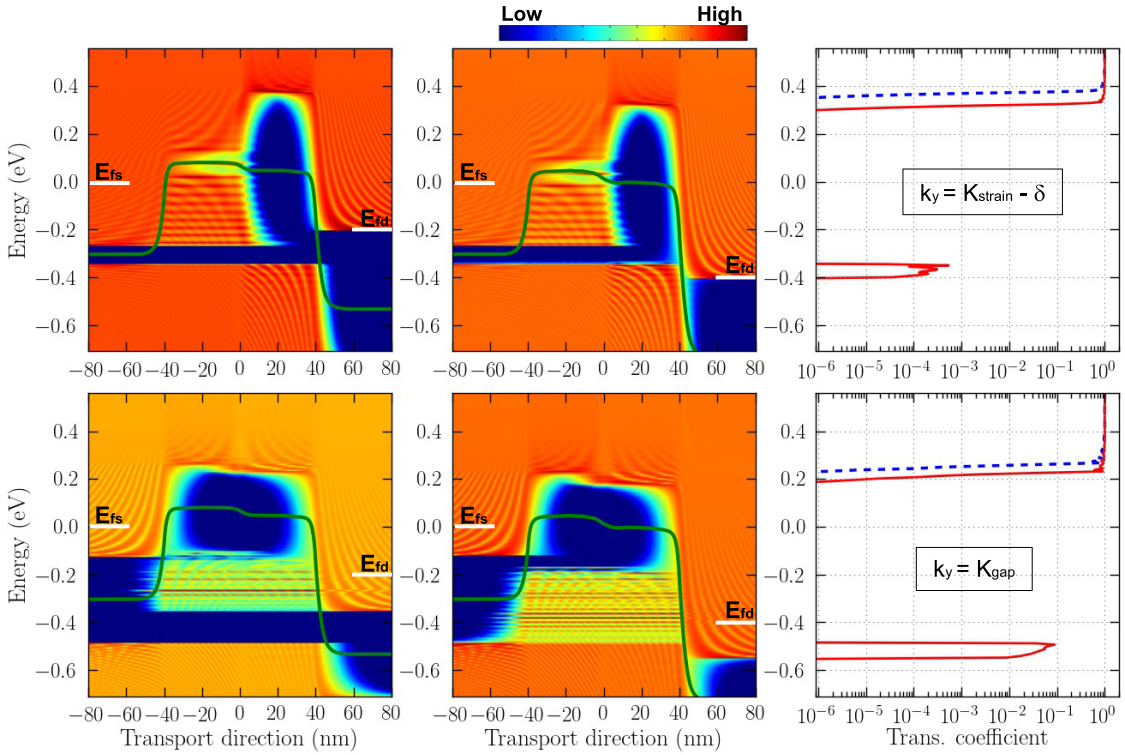


**Figure 4.** Local density of states (left and middle panels) and corresponding transmission coefficient (right panels) for two different wavevectors $k_y$ in the OFF state ($V_{gs} = -0.1$ V) of the nFETs studied in figure 3(b). The values $K_{strain}$ and $K_{gap}$ are defined as in figure 2(b), while $\delta = 0.005\pi/L_y$. The drain voltage $V_{ds} = 0.2$ (resp. 0.4) V in the left (resp. middle) panels, which corresponds to the dashed (resp. solid) lines of the transmission coefficient in the right panels. The source and drain Fermi levels $E_{fs,fd}$ are indicated and the potential profile at the neutrality point is superimposed in the left and middle panels.

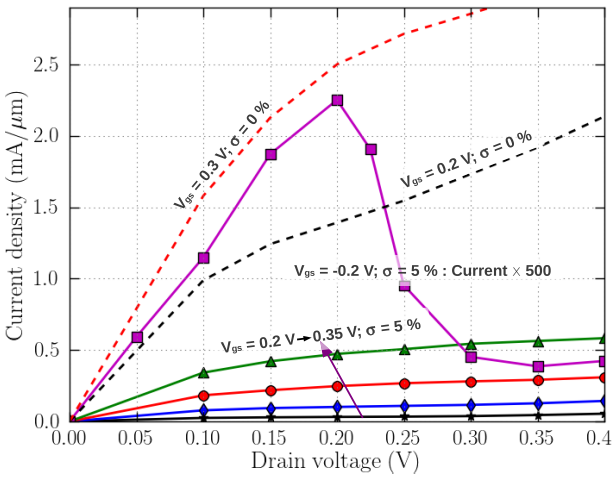


**Figure 5.** $I$–$V_{ds}$ characteristics of simulated graphene nFETs with different $V_{gs}$: unstrained graphene channel ($\sigma = 0\%$) and strained graphene heterostructure ($\sigma = 5\%$). Note that the current at $V_{gs} = -0.2$ V is multiplied by 500.

$V_{gs} = V_{ds} = 0.3$ V, while it is about 13.9 mS $\mu m^{-1}$ in the unstrained case.

Combined with the high transconductance, the good saturation of current in the positive $V_{gs}$-range would be expected to result in a high value of voltage gain $A_v = g_m/g_d$, where $g_d$ is the output conductance. In figure 5, we display the current as a function of drain voltage in the $V_{gs}$-range from 0.2 to 0.35 V. Indeed, the saturation behavior of current is significantly improved when using strained hetero-channels, compared to the unstrained graphene FETs. As a consequence of the reduced output conductance, the voltage gain at $V_{ds} = 0.3$ V reaches values of ~9.5 and 18 for $V_{gs} = 0.2$ V and 0.3 V, respectively, while it is only ~2.8 and 4.7 in the unstrained device. To further evaluate the operation of the device in the high-frequency range, we estimate the cut-off frequency $f_T$ and the maximum oscillation frequency $f_{max}$ using the standard expressions $f_T = g_m/2\pi C_G$ and $f_{max} = f_T/\alpha$, with $\alpha = 2\sqrt{g_d(R_S + R_G) + g_m R_G C_{GD}/C_G}$ [49]. $C_G$ and $C_{GD}$ are the total gate and gate-to-drain capacitances while $R_S$ and $R_G$ are the source and gate resistances, respectively. We take the values of $R_S$ and $R_G$ reported in [49, 50], where $R_S$ is typically ~100 Ω $\mu$m and $R_G$ reasonably reaches a value of 200 Ω $\mu$m. For $V_{gs} = V_{ds} = 0.3$ V, we obtain $f_T \simeq 290$ GHz, while $f_{max} \simeq 304$ GHz is even slightly larger than $f_T$. Similar behaviors have also been reported in some experiments [49, 51]. The corresponding values obtained in the unstrained case are $f_T \simeq 898$ GHz and $f_{max} \simeq 356$ GHz. Thus, although reduced in the strained hetero-channel device, the transconductance and transition frequencies are still high. Together with the good current saturation and consequent high voltage gain, our results demonstrate that the strained hetero-channel devices are also very promising for high-frequency applications.

Finally, we also found that the graphene TFETs can exhibit very strong nonlinear effects in the $I$–$V_{ds}$ characteristics. In

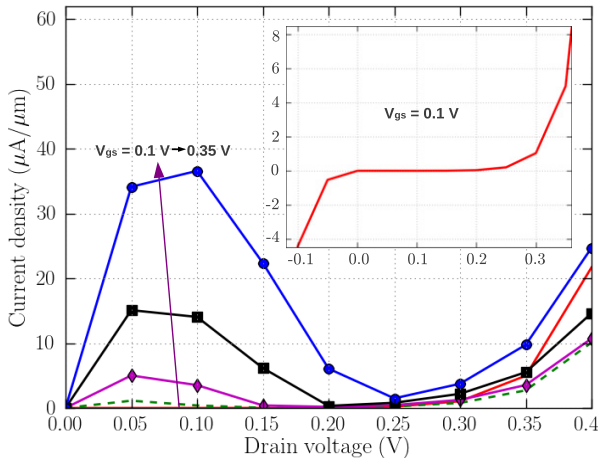


**Figure 6.** $I$–$V_{ds}$ characteristics of simulated graphene TFETs ($\sigma = 5\%$) for $V_{gs}$ ranging from 0.1 to 0.35 V. The inset shows the current, with strong rectification at $V_{gs} = 0.1$ V.

particular, two specific features, namely, a gate-controllable negative differential conductance and strong rectification of current, are observed, as shown in figure 6. Actually, the gate-controllable NDC behavior in TFETs based on a gapped graphene channel has been discussed and explained in [52] by assuming the possibility of controlling the gap profile in the gated zone. Here, our simulations show that the strong NDC behavior can be achieved in the ON state with a peak-to-valley ratio of a few tens (e.g., 47 for $V_{gs} = 0.3$ V). Moreover, because of the strong effects of energy gaps, a finite gap of current occurs in/around the OFF state. This leads to a high ON/OFF current ratio in a finite range of $V_{ds}$, similar to that in the graphene nFETs discussed above, with the possibility of strongly tuning the nonlinearity of the $I$–$V_{ds}$ curves using the gate voltage. It also results in a strong effect of current rectification around $V_{ds} = 0$, as clearly seen in the inset of figure 6. These nonlinear effects can offer great potential for applications such as oscillators, frequency multipliers, fast switching [53], recently proposed non-Boolean logic circuits [54] and rectifier circuits.

## 4. Conclusion

In summary, we have investigated the effects of strain on the transport properties of unstrained/strained graphene heterostructures and considered the possibility of using such heterostructures to improve the performance of graphene transistors. It was shown that, due to deformation of the electronic bandstructure, the mismatch between transport modes having different effective energy gaps in strained/unstrained sections results in a finite conduction gap in these graphene hetero-channels. We have demonstrated that this type of hetero-channel can very significantly improve the performance of graphene FETs for electronic applications. In particular, an ON/OFF current ratio higher than $10^5$ can be achieved. In graphene nFETs, while transconductance and transition frequencies are still high, the performance is additionally improved with respect to conventional graphene FETs in terms of current saturation and the consequent voltage gain. In graphene TFETs, low subthreshold swings and strong nonlinear effects such as gate-controllable NDC behavior and current rectification are observed. This type of strain-induced conduction-gap engineering could certainly be useful for improving the performance of other devices based on graphene/graphene-like materials and for other applications.

## Acknowledgments

V H Nguyen and H V Nguyen thank Vietnam's National Foundation for Science and Technology Development (NAFOSTED) for financial support under Grant no. 103.02-2012.42. P Dollfus acknowledges the French ANR for financial support under the projects NANOSIM-GRAPHENE (Grant no. ANR-09-NANO-016) and MIGRAQUEL (Grant no. ANR-10-BLAN-0304).

## References

[1] Castro Neto A H, Guinea F, Peres N M R, Novoselov K S and Geim A K 2009 The electronic properties of graphene *Rev. Mod. Phys.* **81** 109–62
[2] Schwierz F 2010 Graphene transistors *Nature Nanotechnol.* **5** 487–96
[3] Wu Y, Farmer D, Xia F and Avouris P 2013 Graphene electronics: materials, devices, and circuits *Proc. IEEE* **101** 1620–37
[4] Bolotin K I, Sikes K J, Jiang Z, Klima M, Fudenberg G, Hone J, Kim P and Stormer H L 2008 Ultrahigh electron mobility in suspended graphene *Solid State Commun.* **146** 351–5
[5] Zomer P J, Dash S P, Tombros N and van Wees B J 2011 A transfer technique for high mobility graphene devices on commercially available hexagonal boron nitride *Appl. Phys. Lett.* **99** 232104
[6] Novoselov K S, Geim A K, Morozov S V, Jiang D, Zhang Y, Dubonos S V, Grigorieva I V and Firsov A A 2004 Electric field effect in atomically thin carbon films *Science* **306** 666–9
[7] Wu Y *et al* 2012 State-of-the-art graphene high-frequency electronics *Nano Lett.* **12** 3062–7
[8] Cheng R, Bai J, Liao L, Zhou H, Chen Y, Liu L, Lin Y-C, Jiang S, Huang Y and Duan X 2012 High-frequency self-aligned graphene transistors with transferred gate stacks *Proc. Natl Acad. Sci. USA* **109** 11588–92
[9] Guo Z *et al* 2013 Record maximum oscillation frequency in *C*-face epitaxial graphene transistors *Nano Lett.* **13** 942–7
[10] Meric I, Han M Y, Young A F, Ozyilmaz B, Kim P and Shepard K L 2008 Current saturation in zero-bandgap, top-gated graphene field-effect transistors *Nature Nanotechnol.* **3** 654–9
[11] Han M Y, Özyilmaz B, Zhang Y and Kim P 2007 Energy band-gap engineering of graphene nanoribbons *Phys. Rev. Lett.* **98** 206805
[12] Kharche N and Nayak S K 2011 Quasiparticle band gap engineering of graphene and graphone on hexagonal boron nitride substrate *Nano Lett.* **11** 5274–8
[13] Lherbier A, Botello-Mndez A R and Charlier J-C 2013 Electronic and transport properties of unbalanced sublattice N-doping in graphene *Nano Lett.* **13** 1446–50
[14] Bai J, Zhong X, Jiang S, Huang Y and Duan X 2010 Graphene nanomesh *Nature Nanotechnol.* **5** 190–4

[15] Zhang Y, Tang T-T, Girit C, Hao Z, Martin M C, Zettl A, Crommie M F, Shen Y R and Wang F 2009 Direct observation of a widely tunable bandgap in bilayer graphene *Nature* **459** 820–3

[16] Querlioz D, Apertet Y, Valentin A, Huet K, Bournel A, Galdin-Retailleau S and Dollfus P 2008 Suppression of the orientation effects on bandgap in graphene nanoribbons in the presence of edge disorder *Appl. Phys. Lett.* **92** 042108

[17] Nguyen V H, Chung Nguyen M, Nguyen H-V and Dollfus P 2013 Disorder effects on electronic bandgap and transport in graphene-nanomesh-based structures *J. Appl. Phys.* **113** 013702

[18] Fiori G and Iannaccone G 2009 On the possibility of tunable-gap bilayer graphene FET *IEEE Electron Device Lett.* **30** 261–4

[19] Lee C, Wei X, Kysar J W and Hone J 2008 Measurement of the elastic properties and intrinsic strength of monolayer graphene *Science* **321** 385–8

[20] Sharma B K and Ahn J-H 2013 Graphene based field effect transistors: efforts made towards flexible electronics *Solid-State Electron.* **89** 177–88

[21] Kim K S, Zhao Y, Jang H, Lee S Y, Kim J M, Kim K S, Ahn J-H, Kim P, Choi J-Y and Hong B H 2009 Large-scale pattern growth of graphene films for stretchable transparent electrodes *Nature* **457** 706–10

[22] Lu Y and Guo J 2010 Band gap of strained graphene nanoribbons *Nano Res.* **3** 189–99

[23] Cocco G, Cadelano E and Colombo L 2010 Gap opening in graphene by shear strain *Phys. Rev.* B **81** 241412

[24] Pereira V M and Castro Neto A H 2009 Strain engineering of graphene's electronic structure *Phys. Rev. Lett.* **103** 046801

[25] Huang M, Yan H, Heinz T F and Hone J 2010 Probing strain-induced electronic structure change in graphene by Raman spectroscopy *Nano Lett.* **10** 4074–9

[26] Bunch J S, van der Zande A M, Verbridge S S, Frank I W, Tanenbaum D M, Parpia J M, Craighead H G and McEuen P L 2007 Electromechanical resonators from graphene sheets *Science* **315** 490–3

[27] Kumar S B and Guo J 2012 Strain-induced conductance modulation in graphene grain boundary *Nano Lett.* **12** 1362–6

[28] Pereira V M, Castro Neto A H, Liang H Y and Mahadevan L 2010 Geometry, mechanics, and electronics of singular structures and wrinkles in graphene *Phys. Rev. Lett.* **105** 156603

[29] Pellegrino F M D, Angilella G G N and Pucci R 2010 Strain effect on the optical conductivity of graphene *Phys. Rev.* B **81** 035411

[30] Guinea F, Katsnelson M I and Geim A K 2010 Energy gaps and a zero-field quantum Hall effect in graphene by strain engineering *Nature Phys.* **6** 30–3

[31] Low T and Guinea F 2010 Strain-induced pseudomagnetic field for novel graphene electronics *Nano Lett.* **10** 3551–4

[32] Zhai F and Yang L 2011 Strain-tunable spin transport in ferromagnetic graphene junctions *Appl. Phys. Lett.* **98** 062101

[33] Bunch J S, Verbridge S S, Alden J S, van der Zande A M, Parpia J M, Craighead H G and McEuen P L 2008 Impermeable atomic membranes from graphene sheets *Nano Lett.* **8** 2458–62

[34] Bao W, Miao F, Chen Z, Zhang H, Jang W, Dames C and Lau C N 2009 Controlled ripple texturing of suspended graphene and ultrathin graphite membranes *Nature Nanotechnol.* **4** 562–6

[35] Tomori H, Kanda A, Goto H, Ootuka Y, Tsukagoshi K, Moriyama S, Watanabe E and Tsuya D 2011 Introducing nonuniform strain to graphene using dielectric nanopillars *Appl. Phys. Express* **4** 075102

[36] Georgiou T, Britnell L, Blake P, Gorbachev R V, Gholinia A, Geim A K, Casiraghi C and Novoselov K S 2011 Graphene bubbles with controllable curvature *Appl. Phys. Lett.* **99** 093103

[37] Lu J, Neto A C and Loh K P 2012 Transforming moire blisters into geometric graphene nano-bubbles *Nature Commun.* **3** 823

[38] Kase T and Ogino T 2013 Strain in graphene sheets attached to a porous alumina membrane *J. Phys. Chem.* C **117** 15991–5

[39] Lu Y and Guo J 2010 Local strain in tunneling transistors based on graphene nanoribbons *Appl. Phys. Lett.* **97** 073105

[40] Fujita T, Jalil M B A and Tan S G 2010 Valley filter in strain engineered graphene *Appl. Phys. Lett.* **97** 043508

[41] de Juan F, Cortijo A, Vozmediano M A H and Cano A 2011 Aharonov–Bohm interferences from local deformations in graphene *Nature Phys.* **7** 810–5

[42] Bahamon D A and Pereira V M 2013 Conductance across strain junctions in graphene nanoribbons *Phys. Rev.* B **88** 195416

[43] Pereira V M, Castro Neto A H and Peres N M R 2009 Tight-binding approach to uniaxial strain in graphene *Phys. Rev.* B **80** 045401

[44] Blakslee O L, Proctor D G, Seldin E J, Spence G B and Weng T 1970 Elastic constants of compression-annealed pyrolytic graphite *J. Appl. Phys.* **41** 3373–82

[45] Nguyen V H, Mazzamuto F, Bournel A and Dollfus P 2012 Resonant tunnelling diodes based on graphene/h-BN heterostructure *J. Phys. D: Appl. Phys.* **45** 325104

[46] Alarcon A, Nguyen V H, Berrada S, Querlioz D, Saint-Martin J, Bournel A and Dollfus P 2013 Pseudosaturation and negative differential conductance in graphene field-effect transistors *IEEE Trans. Electron Devices* **60** 985–91

[47] Berrada S, Nguyen V H, Querlioz D, Saint-Martin J, Alarcon A, Chassat C, Bournel A and Dollfus P 2013 Graphene nanomesh transistor with high on/off ratio and good saturation behavior *Appl. Phys. Lett.* **103** 183509

[48] Seabaugh A C and Zhang Q 2010 Low-voltage tunnel transistors for beyond CMOS logic *Proc. IEEE* **98** 2095–110

[49] Farmer D B, Valdes-Garcia A, Dimitrakopoulos C and Avouris P 2012 Impact of gate resistance in graphene radio frequency transistors *Appl. Phys. Lett.* **101** 143503

[50] Xia F, Perebeinos V, Lin Y-M, Wu Y and Avouris P 2011 The origins and limits of metal-graphene junction resistance *Nature Nanotechnol.* **6** 179–84

[51] Wu Y Q, Farmer D, Valdes-Garcia A, Zhu W J, Jenkins K A, Dimitrakopoulos C, Avouris P and Lin Y M 2011 Record high RF performance for epitaxial graphene transistors *IEDM Tech. Dig.* p 528

[52] Nguyen V H, Niquet Y M and Dollfus P 2012 Gate-controllable negative differential conductance in graphene tunneling transistors *Semicond. Sci. Technol.* **27** 105018

[53] Mizuta H and Tanoue T 1995 *The Physics and Applications of Resonant Tunneling Diodes* (Cambridge: Cambridge University Press)

[54] Liu G, Ahsan S, Khitun A G, Lake R K and Balandin A A 2013 Graphene-based non-Boolean logic circuits *J. Appl. Phys.* **114** 154310